Heliyon 10 (2024) e27996

Contents lists available at ScienceDirect

Heliyon

journal homepage: www.cell.com/heliyon

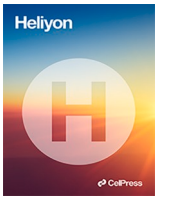

Research article

# Whole transcriptome scanning and validation of negatively related genes in UC-MSCs

Linghan Tian [a,b,c,1], Weibin Wang [d,e,1], Xuzhen Li [d,e], Yan Chen [a,b,c], Qian Song [a,b,c], Lu Yuan [a,b,c], Tingting Hao [d,e], Jiaming Gu [a,b,c], Jian Dong [a,b,c,*]

[a] Department of Yunnan Tumor Research Institute, Kunming, 650118, China
[b] The Third Affiliated Hospital of Kunming Medical University, Kunming, 650118, China
[c] Yunnan Cancer Hospital, Kunming, 650118, China
[d] State Key Laboratory for Conservation and Utilization of Bio-Resources in Yunnan, Yunnan Agricultural University, Kunming, 650201, China
[e] Yunnan Research Institute for Local Plateau Agriculture and Industry, Kunming, 650201, China

ARTICLE INFO

*Keywords:*
Stem cells
UC-MSCs
Differentiation
Stemness
Umbilical cord

ABSTRACT

*Background:* Human umbilical cord mesenchymal stem cells (UC-MSCs) are one of the most extensively researched stem cell types due to their potential for multi-lineage differentiation, secretion of regenerative factors, modulations of immunological activities, and the release of regenerative substances and influence immunological processes. Since UC-MSCs must be cultivated on a large scale for clinical use, selecting the appropriate storing passage, such as the usage-based passage of UC-MSCs, is critical for long-term autologous or allogeneic usage. Long-term cultivation of stem cells, on the other hand, causes them to lose their pluripotent differentiation capacity. As a result, distinguishing between high and low passages of UC-MSCs and identifying the particular variations associated with stem cells and their modes of action is essential for regenerative medicine. Therefore, we investigated the biological features and transcriptional changes of UC-MSCs over passages.

*Methods:* UC-MSCs were isolated from the tissues of the human umbilical cord, and UC-MSCs from five passages (P1, P3, P5, P10 and P15) with three repetitions were compared and identified based on morphology, cell markers, differentiation capacity, and aging-related characteristics. It was previously assumed that the phenotype of cells before the P10 passage was stable, defined as early passage, and that culture could be continued until the 15th passage, defined as late passage. Next, the five passages of UC-MSCs were sequenced using high-throughput complete transcriptome sequencing. Fuzzy C-Means Clustering (FCM) and Weighted Gene Co-expression Network Analysis (WGCNA) were used to find hub genes, and gene silencing was performed to investigate the impact of missing genes on the stemness of UC-MSC cells.

*Results:* UC-MSCs of different passages displayed similar surface markers, including *CD73*, *CD105*, *CD90*, *CD34*, *CD45* and *HLA-DR*. However, the proliferation time of late-phase UC-MSCs was longer than that of early-phase UC-MSCs, and the expression of the senescence-associated (SA)-β-gal staining marker was higher. At the same time, pluripotency markers (*NANOG*, *OCT4*, *SOX2* and *KIF4A*) were down-regulated, and the multi-differentiation potential was reduced.

* Corresponding author. The Third Affiliated Hospital of Kunming Medical University, Kunming, 650118, China.
*E-mail addresses:* TLHck37@126.com (L. Tian), wangwb@dongyang-lab.org (W. Wang), jasonlixuzhen@gmail.com (X. Li), chenyanyn@163.com (Y. Chen), songqian0917@163.com (Q. Song), yl15912073042@163.com (L. Yuan), haott@dongyang-lab.org (T. Hao), Gu1273537057@163.com (J. Gu), dongjian18@yahoo.com (J. Dong).
[1] These authors contributed equally.

https://doi.org/10.1016/j.heliyon.2024.e27996
Received 21 April 2023; Received in revised form 27 February 2024; Accepted 10 March 2024
Available online 12 March 2024

Meanwhile, *KIFC1* and *UBE2C* were down-regulated in late-phase UC-MSCs, which were involved in the maintenance of stemness.
*Conclusions: KIFC1* and *UBE2C* were highly expressed in early-UC-MSCs and showed a downward gradient trend with cell expansion *in vitro*. They regulated UC-MSC proliferation, colony sphere formation, multiple differentiation, stemness maintenance, and other biological manifestations. Therefore, they are anticipated to be new biomarkers for UC-MSCs quality identification in regenerative medicine applications.

## 1. Introduction

Mesenchymal Stem Cells (MSCs) are typical multipotent stem/stromal cells that have the potential to differentiate into various cell types. They can be isolated from various sources, such as bone marrow, umbilical cord, dental pulp, adipose tissue, Wharton's jelly, placenta, fetal viscera or skeletal tissues [1]. MSCs have the ability to self-renew and secrete various trophic factors, making them extensively applied in cell-based therapy [2–6]. Although bone marrow stem cells were the first MSCs to be used and extensively investigated, their use began to decrease due to the cost-intensive progress for fruitless extraction. UC-MSCs showed more rapid proliferation than cells derived from other tissues [7]. Compared with other MSCs, UC-MSCs have been regarded as an excellent source for their ease to harvest, low immunogenicity, and innate homing ability [8].

However, the long-term culture of UC-MSCs could lead to replicative senescence and the reduction or loss of pluripotency. Senescence has been implicated in the loss of stemness, ultimately leading to a gradual decrease in proliferation potential and impaired function. The MSCs have a spindly and plump appearance with a dense network of microvilli when cultured *in vitro* [9]. The ability of MSCs to proliferate is significantly reduced after ten passages [10,11]. Then, in the middle and late stages of culture, the cells become wider, flatter, and extend a large number of pseudopodia (the 11th and 17th passages). The number and length of microvilli are also reduced [9]. Moreover, trypsin during subculture irreversibly damages the structure of MSCs surface, which may be the primary cause of cell morphological changes and decreased proliferation activity caused by *in vitro* culture [12,13]. The previous differentially expressed genes (DEGs) analysis of human MSCs harvested in the 3rd, 5th, and 7th passages revealed that 40% of the significantly expressed genes are related to cell growth, proliferation, and development, demonstrating that *in vitro* passage culture could significantly affect gene expression related to MSCs growth and proliferation due to a lack of nutrition and support from the internal microenvironment [14,15].

The International Society for Cell and Gene Therapy (ISCT) proposed a set of minimum criteria for cell therapy to define MSCs, including cell adhesion under standard culture conditions, poor expression of *CD14*, *CD19*, *CD34*, *CD45*, and *HLA-DR*, and high expression of *CD73*, *CD90* and *CD105*, which maintain the potential of multiline differentiation of osteogenesis, chondrogenesis, and adipogenesis *in vitro* [16]. However, the definition of MSCs remains elusive and has remained debatable for years, particularly in regard to separating and identifying the quality of MSCs from several passages in continuous culture, as there are no distinct criteria.

Therefore, identifying individual deterministic biomarkers makes it difficult to determine the functionality of UC-MSCs, thus limiting their clinical application. Identifying specific biomarkers for long-term culture cells to improve UC-MSC utilization efficiency and reduce detection costs, as well as cell markers that can distinguish the growth stages of UC-MSCs in detail, would be critical. Thus, in this present study, we investigate the biological features, gene expression changes of UC-MSCs over the passages, and the effects of genes that showed a downward trend on stemness and cell passage.

## 2. Materials and methods

### 2.1. Isolation and culture of UC-MSCs

An umbilical cord was obtained from normal pregnant woman immediately after a cesarean section, and cells were separated within 1 h at The First People's Hospital of Yunnan Province. The patient provided signed informed consent (KYLX2023-018) for tissue sampling. The umbilical cord was cut into 2–5 cm tissue segments in a high-sugar DMEM solution using eye scissors. Three blood vessels were stripped off the umbilical cord tissues, while the rest was cut into 1 $mm^3$ pieces. Then, the tissue was resuspended with NutriStem®MSC XF, transferred into culture bottles (Corning,USA), and cultured at 37 °C in a 5% $CO_2$ incubator (Forma ，USA). In primary culture tissues, the cells began to crawl out 5–7 days after culture, and at 11–14 days after culture, cells in most tissues could pass through in large numbers. After UC-MSCs were isolated from the umbilical cord, overexpression of *CD73*, *CD90* and *CD105* but poor expression of *CD34*, *CD45* and *HLA-DR* were observed. In this study, we used six umbilical cords for primary culture of UC-MSCs and subsequent studies.

### 2.2. Evaluation of the three-line differentiation potential and doubling time of UC-MSCs

UC-MSCs were seeded in six-well plates and treated in an adipogenic medium (BI, Israel) for 14–21 days. The medium was replaced every 3–5 days. After lipid droplets were formed, oil red O staining was used to assess adipogenesis. UC-MSCs were seeded in six-well plates to induce osteogenic differentiation and treated in an osteogenic medium (BI, Israel) for 21 days. Similarly, the medium was replaced every 3–5 days, as previously described, Osteogenesis was assessed by alizarin red staining.UC-MSCs were seeded in six-well

plates to induce chondrogenic differentiation and treated in StemPro™ Chondrogenesis Differentiation Kit (Gibco, USA) for 14 days. Differentiated cells were confirmed by Alican Blue staining, and all photos were taken under a microscope (Laica,GER).

An inverted microscope (Laica,GER) was used daily to track the morphological changes of the UC-MSCs. Inverted microscopy was used daily to track morphological changes in UC-MSCs. To determine the relative doubling time of cells in different cell channels. For this purpose, a defined number of cells were seeded and when cells reached 70–90% confluence, they were separated with 0.05%/0.02% trypsin-EDTA solution (Biochrom). patterson's formula, where t is time (h), N0 is the initial number of cells after inoculation and Nt is the number of cells after t hours of incubation, was used to calculate UC-MSCs at different doubling times at different channel numbers.

### 2.3. Senescence-associated β-galactosidase assay

Cell senescence was determined using a β-galactosidase (β-gal) staining kit (Beyotime, China). UC-MSCs were fixed and stained with the solution at 37 °C for 24 h. Then, cells positive for β-gal activity were observed under a microscope.

### 2.4. RNA extraction and real-time PCR

Total RNA was isolated from UC-MSCs using the TRIzol reagent (Invitrogen, USA). and then reverse transcribed into cDNA using a PrimeScript RT reagent kit (Takara, Japan) according to the kit protocol. Quantitative real-time PCR was performed using the LightCycler FastStart DNA MasterPLUS SYBR Green I Kit (Roche, USA). *RPS13* was used as the control gene. Primers (Supplementary Table 1) were synthesized by TSINGKE Biotechnology (Beijing, China) for specific target genes. Template cDNA was added to the reaction mixture and amplified with a 10-min template denaturation step at 95 °C, followed by 40 cycles of 95 °C and 60 °C for 1 min over 15s (ABI 7500, USA). All experiments were repeated thrice.

### 2.5. Spheroid and colony formation

Cells in good condition were planted in the ultra-low adsorption cell culture plate for cell culture. About 1000 cells were added to each well of the 24-well plate and cultured for about 14 days. The number and size of spherules were measured and counted under a microscope.

### 2.6. Cell counting kit-8 cell proliferation assay

Cells were seeded in 96-well plates at a density of $1 \times 10^3$ cells/well (100μL/well). At the testing time point, 10 μL of CCK-8 solution (Takara, Japan) was added to each experimental well and incubated for 2h at 37 °C. Absorbance was measured at 450 nm with an automatic microplate reader (Tecan, Switzerland).

### 2.7. Transfection of cell lines

KIFC1, UBE2C small interfering RNAs (KIFC1 and UBE2C siRNAs) and negative control siRNAs were chemically synthesized by GEMA and designed with three RNA interfering target sequences. The siRNA (small interfering RNA) sequences are shown in Supplementary Table 2. P3-UC-MSCs cells were seeded and cultured in a growth media until the cell density reached 60% prior to transfection with small interfering RNAs (siRNAs). The Lipofectamine 2000 reagent (Invitrogen, USA) was used for siRNA transfection following the manufacturer's instructions. The culture medium was replaced 6 h post–transfection. The cells were harvested 48h after transfection, and the total RNA was isolated according to the manufacturer's instructions (Roche, Switzerland). Specific silencing of *KIFC1* and *UBE2C* expression was assessed using qRT–PCR.

### 2.8. Surface marker expressions of UC-MSCs by flow cytometry

Flow cytometry (BD, USA) analysis was performed to assay the surface marker expressions of UC-MSCs. Cells in 100 μL PBS (Hyclone, China) were incubated with *CD34*, *CD45*, *CD73*, *CD90*, *CD105* and *HLA-DR* antibodies (BD, USA) conjugated with FITC or PE for 15 min in darkness. The cells were assayed by flow cytometry (BD, USA), and the original data were analyzed using the Flowjo software (version 10).

### 2.9. Statistical analysis

Independent experiments were repeated thrice. The SPSS v20.0 software was used for statistical analysis. All quantitative data are presented as mean ± standard deviation (SD). Nonparametric tests were used to analyze differences between groups. A $p$-value $<0.05$ was considered statistically significant. *$p$ value $< 0.05$ **$p$ value $< 0.01$ ***$p$ value $< 0.001$.

### 2.10. RNA extract, quality control, library preparation, and sequencing

Total RNA extraction, quality control, library preparation, and sequencing of the samples used in this work were all handled by the

Beijing Genomics Institute (BGI) utilizing BGI's standard operating procedures. Initially, the MGIEasy rRNA kit (MGI, China) was used to remove rRNA from the total RNA of 15 pre-extracted samples, and the RNA was fragmented after purification. Then, using the MGIEasy RNA directional library, we prepared the random primer and the reverse transcriptase included in the kit to synthesize the first strand of cDNA, then synthesize double-stranded cDNA with DNA polymerase I and RNaseH. The double-stranded cDNA product was then joined by dA-tailing and adapter. The connecting product was amplified, the PCR product was denatured thermally to form a single strand, and a bridge primer was used to cyclize the single-strand DNA to form a single-strand circular DNA library, which was then sequenced on DNBSEQ (PE100). The sample is shown in Supplementary Table 3.

### 2.11. Clean data preparation and quality controlling

The raw reads obtained through sequencing contained low-quality and contaminated adapters, and the "N" was excessive. It was necessary to use the filtering software SOAPnuke [17], independently developed by BGI, to filter (-l 15 -q 0.2 -n 0.05) to remove reads containing adapter; remove reads with "N" greater than 5%; and remove low-quality reads having a proportion of bases with a mass value less than 15 that is greater than 20% of the total base number of the reads. The "Clean Reads" that have been filtered were saved in FASTQ format.

### 2.12. Alignment and transcript assembly

After obtaining the clean reads, Hisat2 [18] was used to compare the clean reads with the reference genome (–sensitive –no-discordant –no-mixed –I 1 -X 1000 -p 8 –rna-strandness GCF_000001405.39_GRCh38.p13). Bowtie2 (version 2.2.5) [19] was used to compare clean reads to the reference gene sequence (-q –phred64 –sensitive –dpad 0 –gbar 99999999 –mp 1,1 –np 1 –score-min L,0, -0.1 –I 1 -X 1000 –no-mixed –no-discordant -p 1 -k 200). Then, RSEM (version 1.2.12) [20] was used to calculate the expression of genes/transcripts (–forward-prob 0) to quantify the gene/transcript expression in the sample and obtain the FPKM expression matrix.

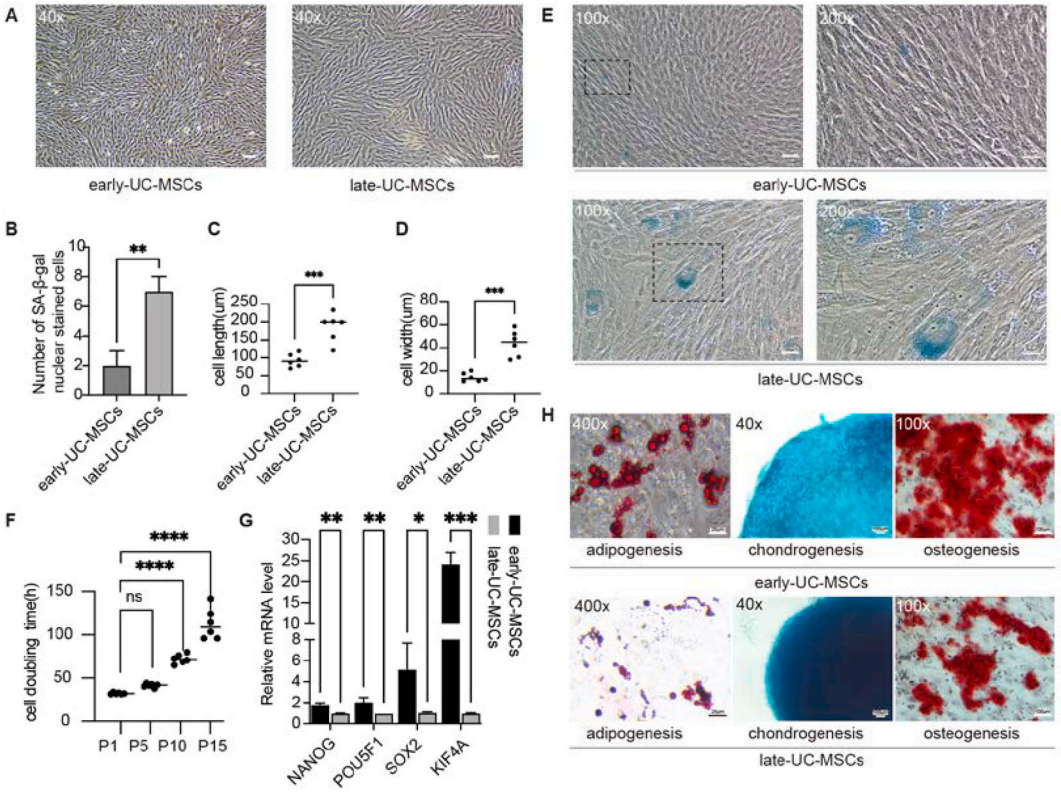


**Fig. 1. Difference of UC-MSCs between early and late passages. A**, cell morphology of early and late passage (40 × ); **B,** Showing the number of SA-β-gal nuclear stained cells**;C& D**, UC-MSCs length and width of early and late passage (μm); **E**, blue staining of the nucleus of senile cell depression under photon microscope (100 × , 200 × ), the black box shows the same area; **F**, doubling times of UC-MSC in each passage; **G**, the expression level of pluripotency markers *NANOG*, *OCT4* (*POU5F1*), *SOX2* and *KIF4A* in the early and late passage of UC-MSCs by PCR; **H**, tests of adipogenesis, chondrogenesis and osteogenesis to examine the differences in multipotency between early and late passages of UC-MSCs. Positive results were obtained using fat droplets stained with Oil Red O. A blue staining indicates the presence of proteins that help to produce extracellular matrix proteoglycans or glycoproteins, known as cartilaginous derivatives. A positive stain reveals the presence of calcium deposits associated with bone mineralization in osteogenic derivatives stained with Alisalin Red.

### 2.13. Fuzzy C-Means Clustering and WGCNA

Based on all the mRNA expression matrix, we averaged the FPKM values of five different periods (P1, P3, P5, P10 and P15) with three repeated experiments as the input and used the Mfuzz software (version 2.56.0) [21] to conduct soft clustering (Fuzzy C-Means Clustering). The Mfuzz default parameters were used to eliminate low-expression genes, processing the missing value and for standardization. The clustering number was 40 (min.acore = 0.4, minimum membership values of a gene belonging to the cluster core). By this, clustering the genes with similar expression patterns was performed. To identify the core expression network, based on the all mRNA expression matrix, Weighted Gene Co-expression Network Analysis (WGCNA) was constructed using the WGCNA algorithm implemented in R WGCNA package (version 1.71) [22] (power = 5, R2 = 0.9, minModuleSize = 30, deepSplit = 2, cutHeight = 0.15). Furthermore, we conducted differential expression analysis on gene sets with obvious and regular downward trends screened by Mfuzz and finally intersected with WGCNA's significant and highly correlated module gene sets to obtain candidate genes for further analysis.

## 3. Results

### 3.1. Differences in morphologies and three-line differentiation potential between the early and late passages of UC-MSCs

UC-MSCs were extracted, grown continuously in a primary medium, and organized into groups based on the passages (Fig. 1A). In this study, we looked at how the cell doubling times of UC-MSCs with various passage numbers changed. P1–P5 have a maximum cell doubling time of 44H, defined as early passage, and P10–P15 have a maximal cell doubling time of 141H, defined as late passage (Fig. 1F). Simultaneously, we noticed that late-UC-MSCs had cells that were noticeably longer and wider than early-UC-MSCs (Fig. 1C–D). To distinguish between early and late passages of UC-MSCs we evaluated the nuclear staining of UC-MSCs from

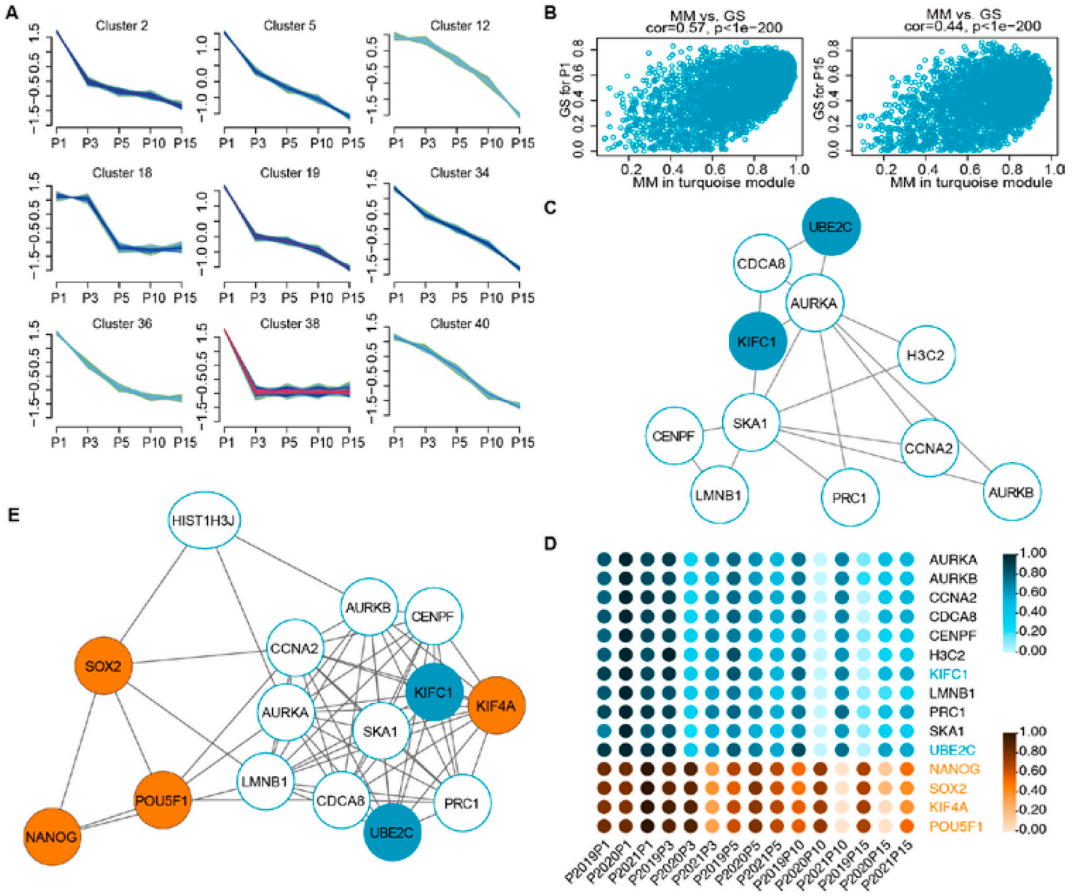


**Fig. 2. WGCNA and FCM of all mRNA. A,** partial FCM of 40 clusterings was down-regulated, and the gene of membership values below 0.4 was eliminated. The x-axis represents the passage while the y-axis represents expression changes; **B**, scatter plot of correlation analysis of MEturquoise and passages (P1 and P15). The higher the correlation between the module MM and the current GS, the more positively the module was correlated with the phase. **C**, the network diagram of the hub gene in a downtrend. **D**, heatmap of hub gene in a downtrend with 3 replicates in 5 periods, *H3C2* and *OCT4* a.k.a HIST1H3J and POU5F1, respectively; **E**, PPI network diagram for the hub and stem gene. As for the detailed data of Fuzzy C-Means Clustering and WGCNA, please refer to Supplementary Fig. 2 and Supplementary Fig. 3.

various passages using senescence-associated β-galactosidase (SA-β-gal). The staining intensity of late-UC-MSCs was higher than that of early-UC-MSCs (Fig. 1E). The flow cytometry analysis of cell surface markers showed that *CD73*, *CD105*, and *CD90* were positive, whereas *CD34*, *CD45*, and *HLA-DR* were negative in both early and late passages of UC-MSCs (Supplementary Fig. 1), but no statistically significant difference was observed between the two groups.

The results showed that both the early and late passage MSCs express particular surface markers that comply with ISCT standards (Supplementary Fig. 1). Next, PCR was used to investigate the expression levels of pluripotency markers (*NANOG, OCT4*, *SOX2*, *KIF4A*; Supplementary Table 1) in the early and late passages of UC-MSCs to further examine the trend of the biological properties of MSCs with increasing culture periods (Fig. 1G). The late-UC-MSC expression levels were significantly lower than those of early-UC-MSCs expression levels, suggesting that the stem cell capacity declined with the growing number of culture passages. We also examined the differentiation capacity of UC-MSCs into adipocytes, chondrocytes, and osteocytes in both early and late passages (Fig. 1H). The results showed that the ability of late-UC-MSCs to differentiate into adipocytes, chondrocytes and osteoblasts was significantly reduced compared to early-UC-MSC. Therefore, we anticipated that following the long-term culture of late-UC-MSCs *in vitro*, some non-expressed or low-expressed genes might impair the self-renewal ability and three-line differentiation potential of UC-MSCs.

### 3.2. Transcriptomic sequencing, FCM and WGCNA of low-passages UC-MSCs

We sequenced a total of 15 samples using the DNBSEQ (PE100) platform, with each sample producing an average of 11.32G Clean Bases (Supplementary Table 4). The average mapping rate of samples to genomes was 96.79% (Supplementary Table 5), and the average mapping rate of comparison gene sets was 59.65% (Supplementary Table 6). Next, we detected 83725 genes, including 19813 mRNA, and based on the expression matrix, the Fuzzy C-Means Clustering method was used to perform soft clustering. Then, we divided 40 gene clusters (Supplementary Fig. 2) based on the expression patterns and further chose 9 clusters with an obvious downtrend (2, 5, 12, 18, 19, 34, 36, 38 and 40) for further analysis (Fig. 2A).

We also performed WGCNA on all mRNA expression matrices to investigate the co-expression network of genes with the downtrend. The WGCNA package's pickSoftThreshold option showed that the optimal *Power* value was 5 (Supplementary Fig. 3A). After obtaining 31 classification modules, similar modules were merged (MEDissThres = 0.15), obtaining 24 modules (Supplementary Figure 3B, D-E), with the grey module representing genes that were not successfully classified. Module Membership (MM) and Gene Significance (GS) analyses of each module in the five stages (P1, P3, P5, P10, P15) were performed to obtain a gene set that was highly related to each growth stage (Fig. 2B). Then, we chose the highly correlated modules in P1 and P15 ($p < 0.05$, $|Cor| > 0.5$) and chose turquoise and light cyan as the target modules (Fig. 2E, Supplementary Fig. 3E). The network was then exported using the WGCNA package's exportNetworkToCytoscapeda option (threshold = 0.5), following which 1125 genes were obtained.

### 3.3. Function enrichment analysis, PPI network and hub gene screening

Subsequent to identifying 1125 genes that intersected with the gene set showing a downtrend, 282 genes were preliminary screened. Then, GO enrichment (p-value cuttoff = 0.05) and KEGG enrichment (p-value cuttoff = 0.05) analyses were performed on these 282 candidate genes and found that 268 and 121 genes were enriched in GO and KEGG terms, respectively. Most genes in the GO

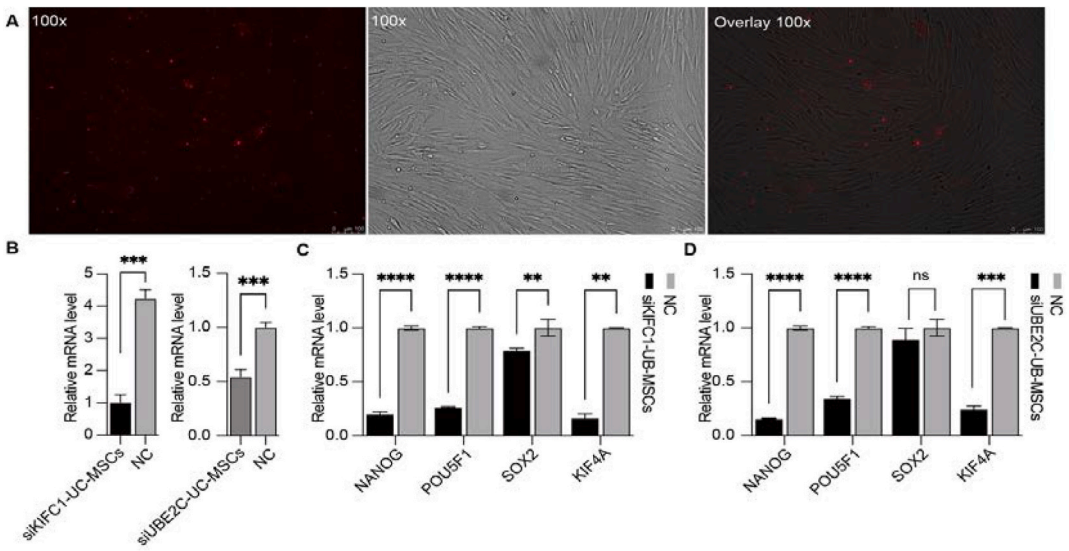


**Fig. 3. Expression pattern of knocked down *UBE2C* and *KIFC*, the knockdown efficiency and pluripotent genes in P3. A**, transfection efficiency under fluorescence microscope and white field (100x); **B**, detection of transfection efficiency by qRT-PCR; **C & D**, qRT-PCR was used to detect the changing relationship of pluripotency markers (*SOX2*, *KIF4A*, *NANOG*, *OCT4* [*POU5F1*], *KIFC1* and *UBE2C*).

terms were found to be enriched in terms related to crucial biological processes such as chromosome aggregation, organelle mission, nuclear division, DNA replication, chromosome aggregation, organelle session, nuclear chromosome aggregation, and so on (Supplementary Fig. 4A). Comparatively, in the KEGG analysis, the most abundant term was cell cycle (hsa04110), followed by alcoholism (hsa05034), neutral extracellular trap formation (hsa04613), systemic lupus thermophilus (hsa05322), and DNA replication (hsa03030) (Supplementary Fig. 4B). The outcomes indicate that the intersection of genes significantly associated with WGCNA in the downtrend primarily consists of genes related to cell cycle, with the expression of genes gradually weakening as the subculture time increases.

Upon integrating the *p*-value with the candidate module and the five periods of growth stage, genes highly correlated with the growth stage of UC-MSCs were further screened, especially the P1 and P15 stages ($|\log FC| \geq 1.5$, MM of METurquose, GS of P1, P3, P5, P10, P15 were$\geq 0.85, \geq 0.5, \geq 0.003, \geq 0.07, \leq -0.15, \leq -0.4$, respectively). Ultimately, 11 hub genes were obtained by intersecting the genes screened by WGCNA with a downtrend (Fig. 2C–Supplementary Table 5), with almost all genes in the network belonging to MEturquoise. After that, 11 hub genes were used in STRING (https://cn.string-db.org/) to build a protein-protein interaction network by default parameter (Fig. 2E). Among the 11 hub genes, we selected two genes, *KIFC1* and *UBE2C*, based on their direct or related interaction with human stemness genes (*NANOG*, *SOX2*, *KIF4A*, and *OCT4*) as the best hub genes (Fig. 2C–E).

### 3.4. Knockdown of UBE2C and KIFC in P3 and the trend of pluripotent gene

We selected *KIFC1* and *UBE2C*, genes with significant variations between late and early passage, using bioinformatics analysis and the qRT-PCR method to further confirm their expression level in three repeats of UC-MSCs of late and early passage (Fig. 3B). Then, after knocking down *KIFC1* (siKIFC1:1.02 ± 0.24; NC:4.24 ± 0.28) and *UBE2C* (siUBE2C:0.55 ± 0.07; NC:1.00 ± 0.05) in P3-UC-MSCs to further investigate their mechanism in UC-MSCs, as well as investigate the correlation between *KIFC1*, *UBE2C* and the genes of pluripotency cell markers (Fig. 3C–D), we observed that the knockdown of *KIFC1* and *UBE2C* altered several typical pluripotent marker genes. Next, qRT-PCR was used to examine the relationship between the expression levels of pluripotency markers (*SOX2*, *KIF4A*, *NANOG* and *OCT4*) with *KIFC1* and *UBE2C*. (Fig. 3C–D).

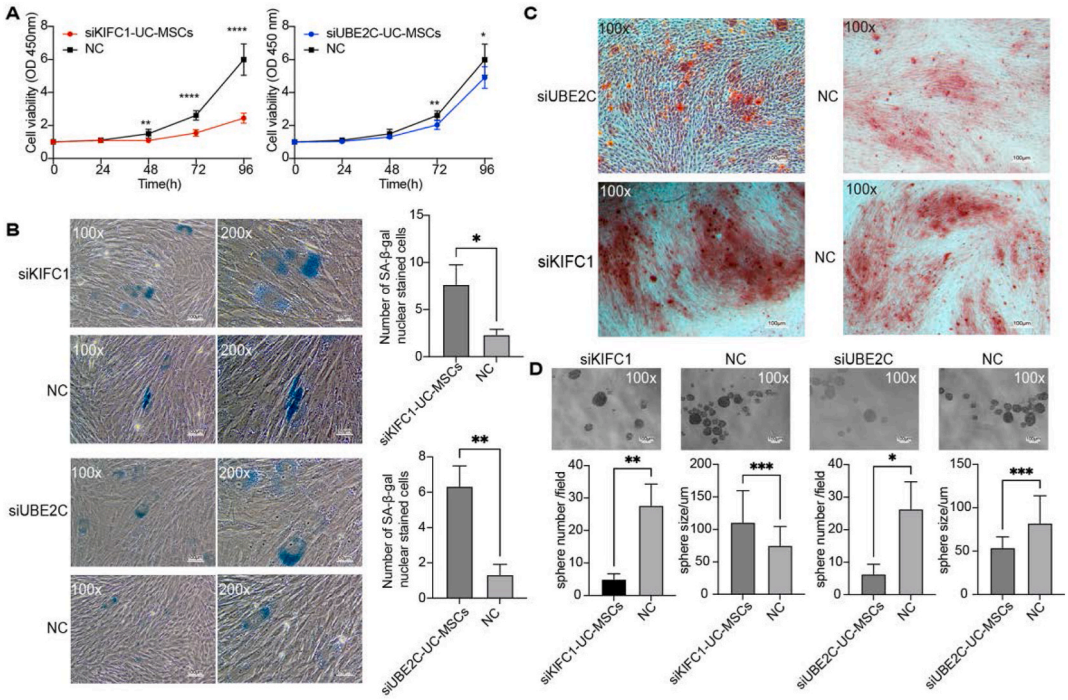


**Fig. 4. P3-UC-MSC behavior and differentiation potential after silencing *UBE2C* and *KIFC1*.** **A**, CCK8 was employed to assess the proliferation of cells from both the experimental and negative control group; **B**, the senescent cells of the experimental group and the negative control group were observed under optical microscopy, showing that the number of blue staining in the same area in the black dashed box in the nucleus (100 × , 200 × ), Showing the number of SA-β-gal nuclear stained cells. **C**, Comparison of the osteogenic ability and difference in multiple differentiation potential between the experimental group and the negative control group (Alisalin Red positive stained osteogenic derivatives indicate the presence of calcium deposits associated with bone mineralization). D, Results of the colony balling test revealed that the pelletizing ability of the control group was better than that of the experimental group.

### 3.5. Knockdowned genes and changes in the biological behavior of UC-MSCs

The effects of the *KIFC1* and *UBE2C* on the three-line differentiation potential and cell stemness of UC-MSCs were discussed in light of the aforementioned data. siRNA was used to target P3-UC-MSCs cells transfected with *KIFC1* or *UBE2C*, respectively. Different levels of slow proliferation were observed in P3-UC-MSCs cells after knocking down *KIFC1* and *UBE2C* (Fig. 4A). Additionally, the number of cells expressing the aging marker SA-β-gal was increased, while the expression of *KIFC1* and *UBE2C* decreased with the lengthening of culture time (Fig. 4B). Further, we discovered a decline in the ability of siKIFC1-UC-MSCs and siUBE2C-UC-MSCs to differentiate into osteoblasts (Fig. 4C). Notably, the spheroid and colony formation of MSCs exhibited varying degrees of loss in siKIFC1-UC-MSCs and siUBE2C-UC-MSCs (Fig. 4D).

## 4. Discussion

MSCs have emerged as a popular area of research in regenerative medicine. The ISCT recommended a single definition of MSCs in 2006, which has since been adopted as the global standard for identifying MSC [16]. Continuous *in vitro* passage is necessary to ensure stem cell yield for clinical applications. However, it is well-known that the function and quality of MSCs from different passages differ to some extent. Moreover, numerous studies have reported that the therapeutic benefits of UC-MSCs at different passages vary in various diseases in different clinical settings [23]. For instance, UC-MSCs with fewer than ten passages have been shown to possess higher cardiogenic differentiation capacity, whereas those with ten to eleven passages exhibited significantly improved neurogenic cell differentiation. Furthermore, UC-MSCs between four and sixteen passages showed a greater osteogenic potential [24]. Additionally, studies have reported that the effects of liver cell homing, proliferation, and apoptosis on the therapy of acute liver failure also vary depending on the passage number [25]. Previous studies have also suggested that at higher passages, MSCs begin to age and exhibit a variety of diminished capacities, including a decline in differentiation and migration [26]. And how to determine the generation with the strongest capacity of MSCs remains controversial. Some single-cell sequencing also confirmed that MSCs exist in stemness subpopulations, functional subpopulations, or proliferative subpopulations, and the function of MSCs mainly depends on the proportion of functional subpopulations at the assessed time point rather than the number of passages, so the marker genes are differentially expressed according to each sample of MSCs, but markers affecting stemness subpopulations, which lead to the changes of the stemness subpopulations and functional subpopulations between the differentiated genes, still need to be further investigated [27].Therefore, maximizing the production of UC-MSCs is a crucial concern for stem cell research.

By combining the phenotypic and functional differences between various passages of UC-MSCs through the research described above, this study aimed to fully analyze the molecular mechanism differences between these passages to make it easier to distinguish their functions and provide new reference biomarkers for clinical use. By comparing the cell phenotypic, surface markers, multi-lineage differentiation, and mRNA expression levels of various UC-MSCs passages, we found that although the surface markers of different UC-MSCs passages were similar, the cell morphology was marginally different, with early passage UC-MSCs exhibiting a more slender cell shape. Furthermore, late-passage UC-MSCs exhibited substantially less osteogenic potential than earlier passages but still retained some multi-lineage differentiation potential. However, the ability of late-passage UC-MSCs to proliferate slowed down, and a large increase in senescent cells was observed.

It is worth noting that the Passages of UC-MSCs cannot be distinguished using the standard definition of the broad surface marker of MSCs, and previous studies have also confirmed that there is no difference in the minimum standards of ISCT definition for P1–P16 generation MSCs [23]. To further investigate the complex internal interactions between Different Passages UC-MSCs, we performed transcriptome analysis and identified a downward gradient tendency in several differentially expressed genes of Various Passages UC-MSCs from P1 to P15. We also performed WGCNA, Fuzzy C-Means Clustering, and differentially expressed gene and interaction network analyses to investigate these interactions. Our results showed that the expression level of *KIFC1* and *UBE2C* in late Passages UC-MSCs were significantly lower than those in early Passages UC-MSCs and showed a downward gradient trend. Interestingly, the PPI protein interaction network revealed strong functional interactions between *KIFC1*, *UBE2C*, and pluripotency markers (*NANOG*, *OCT4*, *SOX2* and *KIF4A*), particularly *KIF4A* (Fig. 2E). We confirmed this association in UC-MSCs using PCR, which was consistent with the quantitative expression data (Fig. 2D–. 3B–D).

Previous studies have suggested that the Kinesin family member C1 (*KIFC1*) is a minus-end-directed motor protein critically involved in microtubule crosslinking and spindle formation [28]. *KIFC1* promotes cellular multipole spindle formation and plays an important role in vesicle and organelle transport, spermatogenesis and neuronal migration to promote the formation of cell spheres [29]. KIFCI is also essential for conserving BLCA stem cells [30]. Recombinant Ubiquitin Conjugating Enzyme E2C (*UBE2C*) is a protein that encodes the disruption of mitotic cyclins and cell cycle processes [31]. *UBE2C* has been implicated in the development of tumor stem cells and was found to be crucial for tumor cell stemness in breast cancer [32] and pancreatic cancer [33]. Studies have also found that *UBE2C* is involved in multiple signaling pathways, including the PI3K-Akt signaling pathway, the toll-like receptor signaling pathway, the TNF signaling pathway, and the MAPK pathway, and plays a key role in dynamic compression-enhanced chondrogenesis [34].

To further investigate the effects of KIFC1 and UBE2C on the phenotypic and functional characteristics of UC-MSCs, we altered their expression levels in P3-UC-MSCs. Our findings indicated that both genes inhibited P3-UC-MSCs proliferation, spheroid colony formation capacity, and multi-lineage differentiation potential to varying degrees while also increasing the fraction of aged cells in P3-UC-MSCs. Additionally, varying extents of reduced pluripotency marker expression, including NANOG, OCT4, SOX2 and KIF4A, as well as KIFC1 and UBE2C were observed (Fig. 3). It was found in this study that *KIFC1* and *UBE2C* are involved in the maintenance of the dry potential of UC-MSCs and that there were differences in their expression in various passages UC-MSCs. *KIFC1* and *UBE2C* are

highly expressed in the early passages of UC-MSCs, which may help distinguish the passages of UC-MSCs and their dry potential, which can provide new ideas for the formulation of quality control reference standards for the clinical use of UC-MSCs.

## 5. Conclusion

We know that multiple passages of UC-MSCs are necessary to ensure expanded production for their clinical applications, but after continuous passages, their differentiation potentials such as phenotype, stemness, proliferation, osteogenesis, and lipogenesis will be altered. In this study, we found that KIFC1 and UBE2C were involved in the maintenance of stemness-associated multidifferentiation potential in UC-MSCs and were differentially expressed in UC-MSCs at different times. The high expression of KIFC1 and UBE2C in early-UC-MSCs will help to distinguish the quality of UC-MSCs and provide new biomarkers for the expansion of UC-MSCs for cell production, storage, and clinical use. providing new biomarkers.

## Ethics approval and informed consent

Written informed consents were acquired from all patients before this study. The protocolof this study was confirmed by the Ethic Committee of Yunnan Cancer Hospital, Yunnan Cancer Hospital and was in compliance with the guidelines of the Declaration of Helsinki.

## Funding statement

Yunnan Province Major Science and Technology Special Project (Biomedicine) “Construction of Yunnan Province Stem Cell Quality Release Detection and Clinical Application Database” (202002AA100006). The Han Weidong Expert Workstation of Yunnan Province, Grant/Award Number: 202105AF150039. Key Laboratory of Cell Therapy Technology Transformation Medicine of Yunnan Province.

## Data availability statement

Data included in article/supp. material/referenced in article.

## CRediT authorship contribution statement

**Linghan Tian:** Methodology, Writing – original draft. **Weibin Wang:** Data curation, Writing – original draft. **Xuzhen Li:** Software, Validation. **Yan Chen:** Investigation. **Qian Song:** Formal analysis, Resources. **Lu Yuan:** Resources. **Tingting Hao:** Data curation. **Jiaming Gu:** Methodology. **Jian Dong:** Project administration, Writing – review & editing.

## Declaration of competing interest

The authors declare that they have no known competing financial interests or personal relationships that could have appeared to influence the work reported in this paper.

## Appendix A. Supplementary data

Supplementary data to this article can be found online at https://doi.org/10.1016/j.heliyon.2024.e27996.

## References

[1] A.J. Friedenstein, Precursor cells of mechanocytes, in: International Review of Cytology, Elsevier, 1976, pp. 327–359.
[2] K.E. Mitchell, M.L. Weiss, B.M. Mitchell, P. Martin, D. Davis, L. Morales, et al., Matrix cells from Wharton’s jelly form neurons and glia, Stem Cell. 21 (2003) 50–60.
[3] L. Zimmerlin, V.S. Donnenberg, J.P. Rubin, A.D. Donnenberg, Mesenchymal markers on human adipose stem/progenitor cells, Cytom Part A 83A (2013) 134–140.
[4] M. Crisan, S. Yap, L. Casteilla, C.-W. Chen, M. Corselli, T.S. Park, et al., A perivascular origin for mesenchymal stem cells in multiple human organs, Cell Stem Cell 3 (2008) 301–313.
[5] R.M. Samsonraj, M. Raghunath, V. Nurcombe, J.H. Hui, A.J. Van Wijnen, S.M. Cool, Concise review: multifaceted characterization of human mesenchymal stem cells for use in regenerative medicine, Stem Cells Transl Med 6 (2017) 2173–2185.
[6] M.F. Pittenger, D.E. Discher, B.M. Péault, D.G. Phinney, J.M. Hare, A.I. Caplan, Mesenchymal stem cell perspective: cell biology to clinical progress, npj Regen Med 4 (2019) 22.
[7] J. Burk, I. Ribitsch, C. Gittel, H. Juelke, C. Kasper, C. Staszyk, et al., Growth and differentiation characteristics of equine mesenchymal stromal cells derived from different sources, Vet. J. 195 (2013) 98–106.
[8] Y. Yu, Y. Song, Y. Chen, F. Zhang, F. Qi, Differentiation of umbilical cord mesenchymal stem cells into hepatocytes in comparison with bone marrow mesenchymal stem cells, Mol. Med. Rep. 18 (2018) 2009–2016.
[9] D. Hladik, I. Höfig, U. Oestreicher, J. Beckers, M. Matjanovski, X. Bao, et al., Long-term culture of mesenchymal stem cells impairs ATM-dependent recognition of DNA breaks and increases genetic instability, Stem Cell Res. Ther. 10 (2019) 218.

[10] A. Otte, V. Bucan, K. Reimers, R. Hass, Mesenchymal stem cells maintain long-term in vitro stemness during explant culture, Tissue Eng. C Methods 19 (2013) 937–948.
[11] P.B. Delben, H.D. Zomer, C. Acordi Da Silva, R.S. Gomes, F.R. Melo, P. Dillenburg-Pilla, et al., Human adipose-derived mesenchymal stromal cells from face and abdomen undergo replicative senescence and loss of genetic integrity after long-term culture, Exp. Cell Res. 406 (2021) 112740.
[12] N.C. Truong, K.H.-T. Bui, P. Van Pham, Characterization of senescence of human adipose-derived stem cells after long-term expansion, in: P.V. Pham (Ed.), Advances in Experimental Medicine and Biology, 2018, pp. 109–128.
[13] H. Azari, M. Rahman, S. Sharififar, B.A. Reynolds, Isolation and expansion of the adult mouse neural stem cells using the neurosphere assay, J Visualized Exp (2010) 2393.
[14] A. Kaminska, A. Wedzinska, M. Kot, A. Sarnowska, Effect of long-term 3D spheroid culture on WJ-MSC, Cells 10 (2021) 719.
[15] I.H. Bellayr, J.G. Catalano, S. Lababidi, A.X. Yang, J.L. Lo Surdo, S.R. Bauer, et al., Gene markers of cellular aging in human multipotent stromal cells in culture, Stem Cell Res. Ther. 5 (2014) 59.
[16] M. Dominici, K. Le Blanc, I. Mueller, I. Slaper-Cortenbach, F.C. Marini, D.S. Krause, et al., Minimal criteria for defining multipotent mesenchymal stromal cells. The International Society for Cellular Therapy position statement, Cytotherapy 8 (2006) 315–317.
[17] Y. Chen, Y. Chen, C. Shi, Z. Huang, Y. Zhang, S. Li, et al., SOAPnuke: a MapReduce acceleration-supported software for integrated quality control and preprocessing of high-throughput sequencing data, GigaScience 7 (2018) 1–6.
[18] D. Kim, B. Langmead, S.L. Salzberg, HISAT: a fast spliced aligner with low memory requirements, Nat. Methods 12 (2015) 357–360.
[19] B. Langmead, S.L. Salzberg, Fast gapped-read alignment with Bowtie 2, Nat. Methods 9 (2012) 357–359.
[20] B. Li, C.N. Dewey, RSEM: accurate transcript quantification from RNA-Seq data with or without a reference genome, BMC Bioinf. 12 (2011) 323.
[21] L. Kumar, M.E. Futschik, Mfuzz: a software package for soft clustering of microarray data, Bioinformation 2 (2007) 5–7.
[22] P. Langfelder, S. Horvath, WGCNA: an R package for weighted correlation network analysis, BMC Bioinf. 9 (2008) 559.
[23] Z. Shi, L. Zhao, G. Qiu, R. He, M.S. Detamore, The effect of extended passaging on the phenotype and osteogenic potential of human umbilical cord mesenchymal stem cells, Mol. Cell. Biochem. 401 (2015) 155–164.
[24] Y.-M. Tang, W.-M. Bao, J.-H. Yang, L.-K. Ma, J. Yang, Y. Xu, et al., Umbilical cord-derived mesenchymal stem cells inhibit growth and promote apoptosis of HepG2 cells, Mol. Med. Rep. 14 (2016) 2717–2724.
[25] X.-J. Song, L. Zhang, Q. Li, Y. Li, F.-H. Ding, X. Li, hUCB-MSC derived exosomal miR-124 promotes rat liver regeneration after partial hepatectomy via downregulating Foxg1, Life Sci. 265 (2021) 118821.
[26] S.H. Hong, M.H. Lee, M.-A. Koo, G.M. Seon, Y.J. Park, D. Kim, et al., Stem cell passage affects directional migration of stem cells in electrotaxis, Stem Cell Res. 38 (2019) 101475.
[27] Z. Xie, W. Yu, G. Ye, J. Li, G. Zheng, W. Liu, et al., Single-cell RNA sequencing analysis of human bone-marrow-derived mesenchymal stem cells and functional subpopulation identification, Exp. Mol. Med. 54 (2022) 483–492.
[28] Y.-X. Xiao, W.-X. Yang, KIFC1: a promising chemotherapy target for cancer treatment? Oncotarget 7 (2016) 48656–48670.
[29] S. Akabane, N. Oue, Y. Sekino, R. Asai, P.Q. Thang, D. Taniyama, et al., KIFC1 regulates ZWINT to promote tumor progression and spheroid formation in colorectal cancer, Pathol. Int. 71 (2021) 441–452.
[30] S. Pan, Y. Zhan, X. Chen, B. Wu, B. Liu, Identification of biomarkers for controlling cancer stem cell characteristics in bladder cancer by network analysis of transcriptome data stemness indices, Front. Oncol. 9 (2019) 613.
[31] L. Yuan, Z. Yang, J. Zhao, T. Sun, C. Hu, Z. Shen, et al., Pan-cancer bioinformatics analysis of gene UBE2C, Front. Genet. 13 (2022) 893358.
[32] Y. Hu, H. Liu, X. Xiao, Q. Yu, R. Deng, L. Hua, et al., Bone marrow mesenchymal stem cell-derived exosomes inhibit triple-negative breast cancer cell stemness and metastasis via an ALKBH5-dependent mechanism, Cancers 14 (2022) 6059.
[33] X. Zhao, H. Li, S. Lyu, J. Zhai, Z. Ji, Z. Zhang, et al., Single-cell transcriptomics reveals heterogeneous progression and EGFR activation in pancreatic adenosquamous carcinoma, Int. J. Biol. Sci. 17 (2021) 2590–2605.
[34] J. Chen, L. Chen, J. Hua, W. Song, Long-term dynamic compression enhancement TGF-β3-induced chondrogenesis in bovine stem cells: a gene expression analysis, BMC Genom Data 22 (2021) 13.